# LEADING EDGE NOISE PREDICTION USING A HYBRID RANS-BEM TECHNIQUE

Paul Croaker, Con Doolan and Nicole Kessissoglou

School of Mechanical and Manufacturing Engineering,

UNSW Australia, Sydney, NSW 2052, Australia

Email: p.croaker@unsw.edu.au

## Abstract

The noise produced by turbulent flow incident on the leading edge of an airfoil is predicted using a hybrid RANS-BEM technique. Hydrodynamic data including turbulent kinetic energy and turbulent dissipation rate are obtained from a steady-state Reynolds Averaged Navier-Stokes (RANS) simulation of turbulent flow past the airfoil. Using a model of the turbulence cross spectrum, statistical noise sources are obtained and then combined with a boundary element method (BEM) model of the airfoil to predict the far-field sound. The results from the hybrid RANS-BEM technique are presented for turbulent flow incident on a NACA0012 airfoil at a Reynolds number based on chord of $Re_c = 6.0 \times 10^5$ and a Mach number of $M = 0.12$. The results are compared with experimental and analytical results from literature.

## 1.  Introduction

Turbulence incident on the leading edge of an airfoil can generate significant noise, often dominating the low frequency sound produced by airfoils and hydrofoils. Amiet [1] developed a leading edge noise model to predict the sound generated by turbulence incident on the leading edge of an airfoil. The method combines a model to determine the pressure jump across a flat plate due to an incident turbulent gust with an acoustic scattering model based on Curle's analogy [2]. Amiet [1] and Paterson and Amiet [3] conducted experiments on the sound generated by a NACA0012 airfoil due to turbulent flow incident on the leading edge. Good agreement was obtained between the experimentally measured sound and the noise predicted using Amiet's leading edge noise model. The derivation of the gust response in Amiet's leading edge noise model assumes that the airfoil is a flat plate. This flat plate assumption will be less accurate for airfoils that are thick or have a non-symmetric profile. Devenport et al. [4] conducted experiments on three airfoil geometries placed in turbulent flow. They found that airfoil thickness dramatically attenuates the high frequency component of the radiated sound field. Angle of attack and camber were found to have only a minor influence on the far-field sound pressure under the assumption of isotropic turbulence.

This paper presents a hybrid RANS-BEM technique to predict flow induced noise produced by turbulent flow past a body. The flow noise sources are modelled using RANS-based statistical noise sources. The incident acoustic field produced by these statistical flow noise sources are then calculated and applied to a BEM-based prediction of the scattering and diffraction. The spatial derivatives are applied to the Green's functions instead of the flow noise sources, hence avoiding any errors associated with numerical differentiation. Using the hybrid RANS-BEM technique, the far-field sound produced by turbulent flow incident on the leading edge of a NACA0012 airfoil at a Reynolds number based on the chord $Re_c$=$6.0 \times 10^5$ and Mach number $M$=0.12 is predicted.

## 2.   Numerical Procedure

### 2.1   Incident Pressure From a Single Turbulent Source

To determine the far-field pressure produced by the scattering of flow induced noise by a rigid body, the incident pressure on the body is calculated using [5]:

$$p_{\text{inc}}\left(\mathbf{x}, \omega\right) = \lim_{\epsilon \to 0} \int_{\left(\Omega - V_\epsilon\right)} \left(\rho_f U_i\left(\mathbf{y}\right) U_j\left(\mathbf{y}\right)\right) \frac{\partial^2 G_h\left(\mathbf{x}, \mathbf{y}\right)}{\partial y_i \partial y_j} d\mathbf{y} \tag{1}$$

where $p_{\text{inc}}\left(\mathbf{x}, \omega\right)$ is the Fourier transform of the incident pressure at field point $\mathbf{x}$ and angular frequency $\omega$. $\rho_f$ is the density of the fluid. $U_i\left(\mathbf{y}\right)$ is the fluid velocity in the $i^{\text{th}}$ direction at the source point $\mathbf{y}$ and consists of a mean component $\bar{U}_i\left(\mathbf{y}\right)$ and a fluctuating component $u_i'\left(\mathbf{y}\right)$ as follows

$$U_i\left(\mathbf{y}\right) = \bar{U}_i\left(\mathbf{y}\right) + u_i'\left(\mathbf{y}\right) \tag{2}$$

$\Omega$ is the computational domain occupied by the flow noise sources and $V_\epsilon$ represents an exclusion neighbourhood around the field point $\mathbf{x}$. This exclusion neighbourhood allows the singularities occurring when $\mathbf{x} = \mathbf{y}$ to be regularised. The harmonic free-field Green's function of the wave equation in three dimensions is given by

$$G_h = \frac{e^{ik_a r}}{4\pi r} \tag{3}$$

and in two dimensions by

$$G_h = \frac{\text{i}}{4} H_0^{(1)}\left(k_a r\right) \tag{4}$$

where $k_a$ is the acoustic wave number, $r = \|\mathbf{x} - \mathbf{y}\|$ is the distance between the source and field points and $\text{i} = \sqrt{-1}$. $H_0^{(1)}$ is a Hankel function of the first kind of order zero. In equation (1), the contribution from viscous stresses has been neglected as only high Reynolds number flows are considered.

In the proceeding derivation, the limit in equation (1) is omitted. The singularity regularisation outlined in Ref. [5] is followed. Decomposing equation (1) into contributions from individual CFD cells produces

$$p_{\text{inc}}\left(\mathbf{x}, \omega\right) = \sum_{c=1}^{C} p_{c,\text{inc}}\left(\mathbf{x}, \omega\right)$$

$$= \sum_{c=1}^{C} \int_{\Omega_c} \left(\rho_f U_{i,c} U_{j,c}\right) \frac{\partial^2 G_h\left(\mathbf{x}, \mathbf{y}\right)}{\partial y_i \partial y_j} d\Omega_c \tag{5}$$

where $p_{c,\text{inc}}\left(\mathbf{x}, \omega\right)$ is the Fourier transform of the incident pressure due to the $c^{\text{th}}$ CFD cell. $U_{i,c}$ is the fluid velocity in the $i^{\text{th}}$ direction at CFD cell $c$. $\Omega_c$ is the computational domain occupied by the $c^{\text{th}}$ CFD cell and $C$ is the total number of CFD cells. Initially considering only two dimensions, assuming the fluid is incompressible and that the velocity is constant over the domain $\Omega_c$, $p_{c,\text{inc}}\left(\mathbf{x}, \omega\right)$ can be represented by

$$p_{c,\text{inc}}\left(\mathbf{x}, \omega\right) = \rho_f \left(U_{1,c}^2\right) \int_{\Omega_c} \frac{\partial^2 G_h\left(\mathbf{x}, \mathbf{y}\right)}{\partial y_1^2} d\Omega_c + 2\rho_f \left(U_{1,c} U_{2,c}\right) \int_{\Omega_c} \frac{\partial^2 G_h\left(\mathbf{x}, \mathbf{y}\right)}{\partial y_1 \partial y_2} d\Omega_c$$

$$+ \rho_f \left(U_{2,c}^2\right) \int_{\Omega_c} \frac{\partial^2 G_h\left(\mathbf{x}, \mathbf{y}\right)}{\partial y_2^2} d\Omega_c \tag{6}$$

Assuming isotropic turbulence, the following approximations for the Lighthill tensor can be used [6]

$$\rho_f \left( U_{1,c}^2 \right) \approx 2\rho_f \bar{U}_{1,c} u'_{s,c}$$
$$\rho_f \left( U_{2,c}^2 \right) \approx 2\rho_f \bar{U}_{2,c} u'_{s,c} \tag{7}$$
$$\rho_f \left( U_{1,c} U_{2,c} \right) \approx \rho_f \bar{U}_{1,c} u'_{s,c} + \rho_f \bar{U}_{2,c} u'_{s,c}$$

where $u'_{s,c}$ is the fluctuating component of the velocity. A velocity normalised incident pressure $\hat{p}_{c,\text{inc}}$ is obtained by dividing the incident pressure $p_{c,\text{inc}}$ by $u'_{s,c}/U_{\text{con}}$, where $U_{\text{con}}$ is the convection velocity, to give

$$\hat{p}_{c,\text{inc}} (\mathbf{x}, \omega) = 2\rho_f U_{\text{con}} \left( \bar{U}_{1,c} \int_{\Omega_c} \frac{\partial^2 G_h (\mathbf{x}, \mathbf{y})}{\partial y_1^2} d\Omega_c + \left( \bar{U}_{1,c} + \bar{U}_{2,c} \right) \int_{\Omega_c} \frac{\partial^2 G_h (\mathbf{x}, \mathbf{y})}{\partial y_1 \partial y_2} d\Omega_c \right.$$
$$\left. + \bar{U}_{2,c} \int_{\Omega_c} \frac{\partial^2 G_h (\mathbf{x}, \mathbf{y})}{\partial y_2^2} d\Omega_c \right) \tag{8}$$

Equation (8) is solved using the near-field formulation for pressure derived previously by the authors and described in detail in Ref. [5].

## 2.2 Scattered Pressure Field using the BEM

The non-homogeneous Helmholtz equation is given by [7]

$$\triangle p_c (\mathbf{x}, \omega) + k_a^2 p_c (\mathbf{x}, \omega) = -Q \tag{9}$$

where $p_c (\mathbf{x}, \omega)$ is the acoustic pressure at field point $\mathbf{x}$ and $Q$ is an acoustic source. A solution of the non-homogeneous Helmholtz equation can be obtained by calculating the incident pressure on the body radiated by the source and applying it as a load to the boundary integral equation as follows [7]

$$c (\mathbf{y}) p_c (\mathbf{y}, \omega) = -\int_\Gamma \frac{\partial G_h (\mathbf{x}, \mathbf{y})}{\partial n (\mathbf{x})} p_c (\mathbf{x}, \omega) \, d\Gamma (\mathbf{x}) + \mathrm{i} \rho_f c_f k_a \int_\Gamma G_h (\mathbf{x}, \mathbf{y}) v_c (\mathbf{x}, \omega) \, d\Gamma (\mathbf{x})$$
$$+ p_{c,\text{inc}} (\mathbf{y}, \omega) \tag{10}$$

where $\Gamma$ is the surface of the body. $c (\mathbf{y})$ is a free-term coefficient equal to 1 in the domain interior and 0.5 on a smooth boundary. $n$ is a unit vector in the direction normal to the boundary. $c_f$ is the speed of sound in the fluid. $v_c$ is the fluid particle velocity and for a rigid surface $v_c = 0$. Using the hybrid RANS-BEM approach, both sides of equation (10) are divided by $u'_{s,c}/U_{\text{con}}$ to yield

$$c (\mathbf{y}) \hat{p}_c (\mathbf{y}, \omega) = -\int_\Gamma \frac{\partial G_h (\mathbf{x}, \mathbf{y})}{\partial n (\mathbf{x})} \hat{p}_c (\mathbf{x}, \omega) \, d\Gamma (\mathbf{x}) + \hat{p}_{c,\text{inc}} (\mathbf{y}, \omega) \tag{11}$$

where $\hat{p}_c$ is the velocity normalised scattered pressure on the body due to the flow noise source in the $c^{\text{th}}$ CFD cell. The velocity normalised scattered pressure in the far-field $\hat{p}_c (\mathbf{x_f}, \omega)$ due to the flow noise source in the $c^{\text{th}}$ CFD cell can be determined by solving

$$\hat{p}_c (\mathbf{x_f}, \omega) = -\int_\Gamma \frac{\partial G_h (\mathbf{x}, \mathbf{y})}{\partial n (\mathbf{x})} \hat{p}_c (\mathbf{x}, \omega) \, d\Gamma (\mathbf{x}) \tag{12}$$

where $\mathbf{x_f}$ is the far-field point. The far-field scattered pressure $p_c (\mathbf{x_f}, \omega)$ can then be obtained by

$$p_c (\mathbf{x_f}, \omega) = \frac{u'_{s,c}}{U_{\text{con}}} \hat{p}_c (\mathbf{x_f}, \omega) \tag{13}$$

A scattered field is obtained for each CFD cell using the AEBEM2 subroutine of Kirkup [8]. AEBEM2 is a two-dimensional BEM solver. As the scattering of sound from turbulent noise sources

is a three-dimensional phenomenon, the scattered pressure calculated by the subroutine must then be converted to three dimensions. The two-dimensional pressure calculated by AEBEM2 is converted into three-dimensional pressure using the following expression [9]

$$p_{c,3D}\left(\mathbf{x_f},\omega\right) \approx p_c\left(\mathbf{x_f},\omega\right) \frac{1+\mathrm{i}}{2}\sqrt{\frac{k_a}{\pi r}} \tag{14}$$

where $p_c\left(\mathbf{x_f},\omega\right)$ and $p_{c,3D}\left(\mathbf{x_f},\omega\right)$ are respectively the two and three-dimensional far-field pressures generated by the scattering of the flow noise sources in the $c^{\text{th}}$ CFD cell.

## 2.3 Far-Field Power Spectral Density

The power spectral density (PSD) $S\left(\mathbf{x_f},\omega\right)$ at the far-field point $\mathbf{x_f}$ is calculated by the double summation as follows

$$S\left(\mathbf{x_f},\omega\right) = \sum_{b=1}^{C}\sum_{c=1}^{C} p_{b,3D}\left(\mathbf{x_f},\omega\right) p_{c,3D}^{*}\left(\mathbf{x_f},\omega\right) \tag{15}$$

where $C$ is the total number of CFD cells and $^*$ indicates the complex conjugate. Substituting equations (13) and (14) into equation (15) yields

$$S\left(\mathbf{x_f},\omega\right) = \sum_{b=1}^{C}\sum_{c=1}^{C} \frac{\Phi(\mathbf{y}_b,\mathbf{y}_c,\omega)}{U_{\text{con}}^2}\frac{k_a}{2\pi r}\left[\hat{p}_b\left(\mathbf{x_f},\omega\right)\hat{p}_c^{*}\left(\mathbf{x_f},\omega\right)\right] \tag{16}$$

where $\Phi(\mathbf{y}_b,\mathbf{y}_c,\omega) = \left[u_{s,b}^{'}u_{s,c}^{'*}\right]$ is the turbulent velocity cross spectrum and is the only unknown quantity in the model.

## 2.4 Turbulent Velocity Cross Spectrum

An analytical model of the turbulent velocity cross spectrum derived by Kerhervé et al. [10] is used here and is given by

$$\Phi(\mathbf{y}_b,\mathbf{y}_c,\omega) = \frac{u_s^2\tau_s}{\sqrt{1+\alpha^2}}\exp\left(-\pi\frac{r_{b,c}^2}{l_s^2\left(1+\alpha^2\right)}\right)\exp\left(-\frac{\omega^2\tau_s^2}{4\pi\left(1+\alpha^2\right)}\right)\exp\left(-\mathrm{i}\omega\frac{\alpha\tau_s r_{b,c}}{l_s\left(1+\alpha^2\right)}\right) \tag{17}$$

where $\alpha = \frac{U_{\text{con}}\tau_s}{l_s}$ and has been set to unity here. $r_{b,c}$ is the distance between the $b^{\text{th}}$ and $c^{\text{th}}$ CFD cells. The model parameters are linked to the RANS simulation at each cell using the following expressions [11]

$$u_s = \sqrt{\frac{2k}{3}}, \qquad \omega_s = \frac{2\pi}{\tau_s}, \qquad \tau_s = \frac{c_\tau k}{\epsilon}, \qquad l_s = \frac{c_l k^{\frac{3}{2}}}{\epsilon} \tag{18}$$

where $k$ is the turbulent kinetic energy and $\epsilon$ is the turbulent dissipation rate. $c_l$ and $c_\tau$ are semi-empirical parameters and have both been assigned a value of unity.

## 2.5 CFD Model

A NACA0012 airfoil with a chord of 230 mm at zero angle of attack was modelled. Amiet et al. [1, 3] conducted experiments on the same airfoil under incident turbulence excitation. Their experimental measurements are used to validate the numerical model and results presented in this paper. In the experiment, the airfoil had a span of 530 mm, however a two-dimensional CFD simulation was performed in this work. Incompressible flow past the airfoil was simulated at a Reynolds number based on chord $Re_c$=6.0$\times 10^5$ and Mach number $M$=0.12. The two-dimensional steady RANS simulation was performed in OpenFOAM on a C-grid domain with approximately 170,000 quadrilateral cells. The boundary layer mesh is well resolved, with $y^+ \sim 1$ for the cells immediately adjacent to the airfoil.

The inlet velocity was set to 40 m/s on the semi-circular boundary. Also, the turbulent kinetic energy and turbulent dissipation rate were artificially increased across a planar region upstream of the airfoil.

The jump in turbulent kinetic energy and dissipation rate were tuned to achieve a turbulence intensity of 4% and length scale of 0.035 m to match the upstream turbulence conditions measured by Paterson and Amiet [3]. A zero average pressure boundary condition was imposed at the outlet. A no-slip condition was applied on the surface of the plate, and the top and bottom boundaries are considered as free-slip walls. The $k - \omega$ SST turbulence model was applied. Figure 1 shows the mesh resolution used in the vicinity of the leading edge.
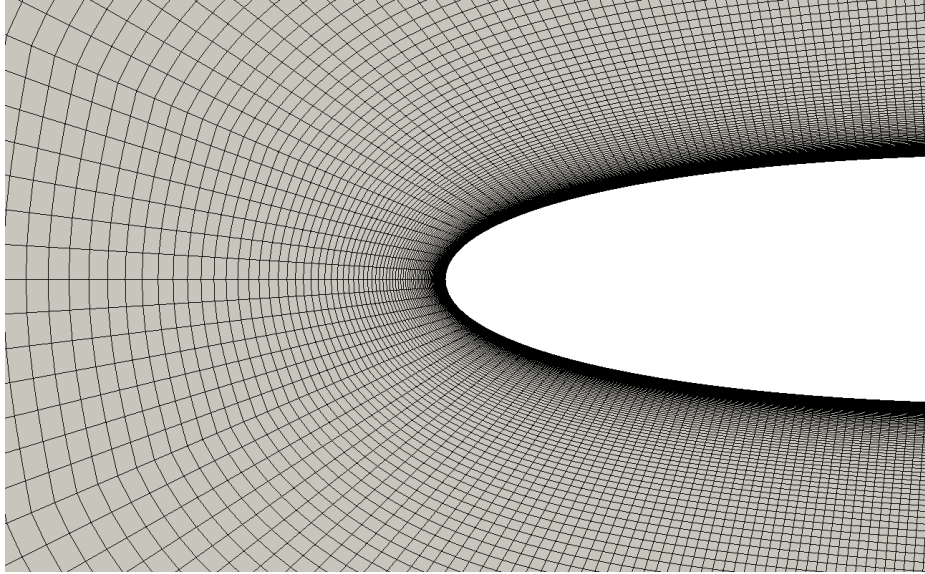


Figure 1 – CFD mesh near leading edge of the airfoil

## 2.6  BEM Model

The two-dimensional BEM model consisted of 580 linear one-dimensional boundary elements distributed around the airfoil. A greater concentration of boundary elements were placed around the leading edge and near the trailing edge to ensure that interaction of the incident field with the geometry of the plate was accurately captured. The vertices of these BEM elements also represent the field points used to calculate the incident normalised pressure using equation (8). The AEBEM2 subroutine of Kirkup [8] was used to solve equation (11) to predict the scattered normalised pressure. Equations (8) and (11) must be solved for each CFD cell. The far-field power spectral density is then calculated using equation (16).

## 3.   Results

## 3.1  Turbulent Flow Field

Figure 2 shows the turbulence intensity (a) and turbulence length scale (b) predicted near the leading edge of the airfoil. Upstream of the leading edge, the turbulence intensity and length scale are approximately 4% and 0.035 m, respectively. These values match the experimental measurements of Paterson and Amiet [3]. In the immediate vicinity of the leading edge, the turbulence intensity increases suddenly. This coincides with a dramatic reduction in the length scale of the turbulence. Santana et al. [12] experimentally observed that the presence of the airfoil induces rapid distortion of the turbulent structures near the leading edge, producing this sudden increase in turbulence intensity and corresponding decrease in turbulence length scale.

Based on the turbulent kinetic energy and dissipation rate, and using the following values for the semi-empirical parameters $c_l = 1.0$ and $c_\tau = 1.0$, the distribution of characteristic velocity $u_s$, characteristic frequency $\omega_s$ and characteristic length $l_s$ used in the RANS-based statistical noise model are calculated. The turbulent velocity cross spectra is then computed using equation (17).

## 3.2  Acoustic Results

The turbulent velocity cross spectra obtained in the preceding section were then applied to the normalised far-field pressures to predict the far-field power spectral density (PSD) given by equation (16). As only

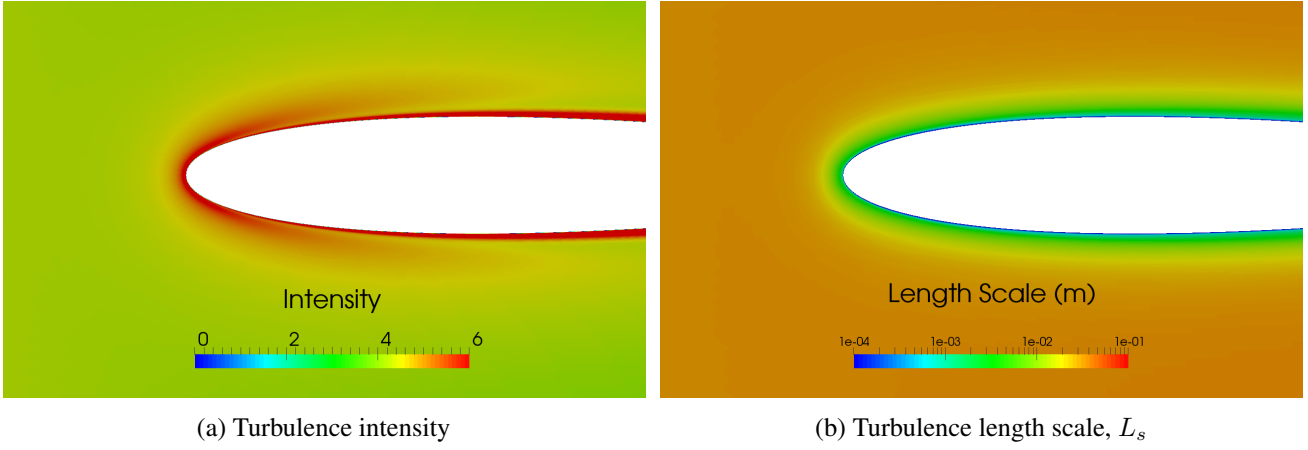(a) Turbulence intensity



(b) Turbulence length scale, $L_s$

Figure 2 – Turbulent properties in the flow near the leading edge

a two-dimensional CFD simulation was performed, the following procedure was adopted to predict the far-field PSD of the 530 mm span:

1. The span was divided into 530 equal segments of 1mm;

2. The far-field PSD of one segment was calculated from equations (13) and (14);

3. The far-field PSD was then modified to account for scattering by the entire span using the following correction [13]

$$\text{PSD}_t = \text{PSD}_s + \text{PSD}_c \tag{19}$$

where $\text{PSD}_t$ and $\text{PSD}_s$ are the power spectral density for the entire span and simulated span, respectively, and $\text{PSD}_c$ is a correction given by

$$\text{PSD}_c = \begin{cases} 10\log\left(N\right), & \frac{L_c^{'}}{L_s} \leq \frac{1}{\sqrt{\pi}} \\ 10\log\left(\frac{L_c^{'}}{L_s}\right) + 10\log\left(\sqrt{\pi}N\right), & \frac{1}{\sqrt{\pi}} < \frac{L_c^{'}}{L_s} < \frac{N}{\sqrt{\pi}} \\ 20\log\left(N\right), & \frac{L_c^{'}}{L_s} \geq \frac{N}{\sqrt{\pi}} \end{cases} \tag{20}$$

where $N$ is the total number of segments. $L_s$ is the length of the simulated span and $L_c^{'}$ is the spanwise coherence length and is approximated by $L_c^{'} = 2.1 U_{\text{con}}/\omega$ [14].

Figure 3 compares the spectrum level of the far-field sound predicted with the hybrid RANS-BEM technique to the experimental measurements and analytical results of Amiet et al. [1, 3]. Here it is assumed that the PSD obtained using the RANS-BEM technique is equivalent to a spectrum level calculated with a 1Hz bandwidth and can hence be directly compared to the results presented by Paterson and Amiet [3]. The far-field sound predicted with the proposed RANS-BEM technique compares favourably with the experimental results at frequencies up to approximately 1.2 kHz. Above this frequency, the difference between the numerical prediction and experimental measurements increases. However, at high frequencies, the signal-to-noise ratio of the experimental results was poor and hence the reliability of the measured sound decreases at high frequencies [1]. The numerical results predicted with the proposed technique also compare well with the leading edge noise model developed by Amiet [1] across the frequency range considered. However it is noted that the leading edge noise model overpredicts the far-field sound at all frequencies.

Figure 4 compares the directivity of the far-field sound predicted with the proposed RANS-BEM technique with experimental measurements [3] and the leading edge noise model of Amiet [1, 3]. In Figure 4, 180 degrees corresponds to the direction of fluid motion over the airfoil. There is excellent agreement between the directivity obtained using the RANS-BEM technique and the experimental measurements at frequencies below 1000 Hz. At higher frequencies, there is a discrepancy between the predicted directivity and the experimental measurement attributed to poor signal-to-noise ratio at these frequencies. At lower frequencies, the directivity pattern has a dipole character and is consistent with scattering from an acoustically compact body. As the frequency increases, multiple lobes that are focused towards the airfoil trailing edge appear. This is consistent with sound scattered by the leading edge being back scattered by the trailing edge to create interference patterns in the directivity plot.
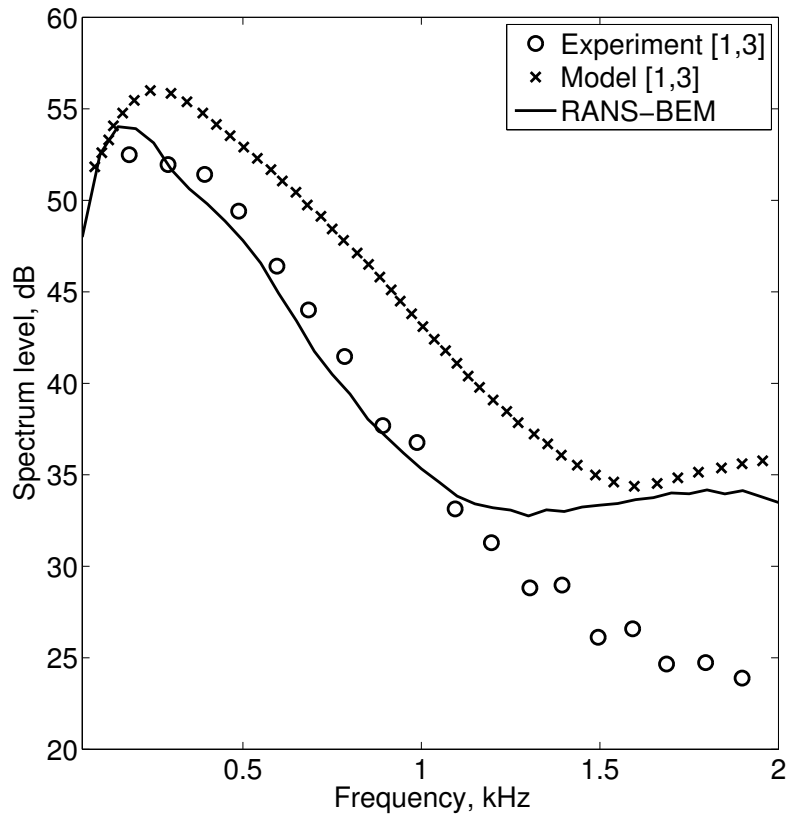
6

Figure 3 – Comparison of numerical and experimental far-field sound

## 4. Summary

A hybrid RANS-BEM technique has been proposed to predict the flow induced noise generated by turbulent flow incident on the leading edge of an airfoil. The method is based on statistical data of the flow over the airfoil as produced by a steady state RANS simulation. The flow field data is processed by a statistical noise model to estimate the turbulent velocity cross spectra. The turbulent velocity cross spectra are then combined with a BEM model to predict the scattering and diffraction of the flow by the leading edge. Application of the hybrid RANS-BEM technique to predict the flow induced noise generated by turbulent flow incident on the leading edge of a NACA0012 airfoil at a Reynolds number based on the chord of $Re_c = 6.0 \times 10^5$ and a Mach number of $M = 0.12$ has been presented. The far-field sound predicted with the proposed RANS-BEM technique was observed to agree well with experimental and analytical results from literature.

## References

[1]   Amiet. R, K, "Acoustic radiation from an airfoil in a turbulent stream", *Journal of Sound and Vibration* 41 (1975), pp. 407–420.

[2]   Curle, N., "The influence of solid boundaries upon aerodynamic sound", *Proceedings of the Royal Society of London. Series A, Mathematical and Physical Sciences* 231 (1955), pp. 505–514.

[3]   Paterson, R. W. and Amiet. R, K, "Noise and surface pressure response of an airfoil to incident turbulence", *Journal of Aircraft* 14 (1977), pp. 729–736.

[4]   Devenport, W. J., Staubs, J. K. and Glegg, S. A. L., "Sound radiation from real airfoils in turbulence", *Journal of Sound and Vibration* 329 (2010), pp. 3470–3483.

[5]   Croaker, P., Kessissoglou, N. and Marburg, S., "Strongly singular and hypersingular integrals for aeroacoustic incident fields", *International Journal for Numerical Methods in Fluids* 77 (2015), pp. 274–318.

[6]   Ffowcs Williams, J. E. and Hall, L. H., "Aerodynamic sound generation by turbulent flow in the vicinity of a scattering half plane", *Journal of Fluid Mechanics* 40 (1970), pp. 657–670.
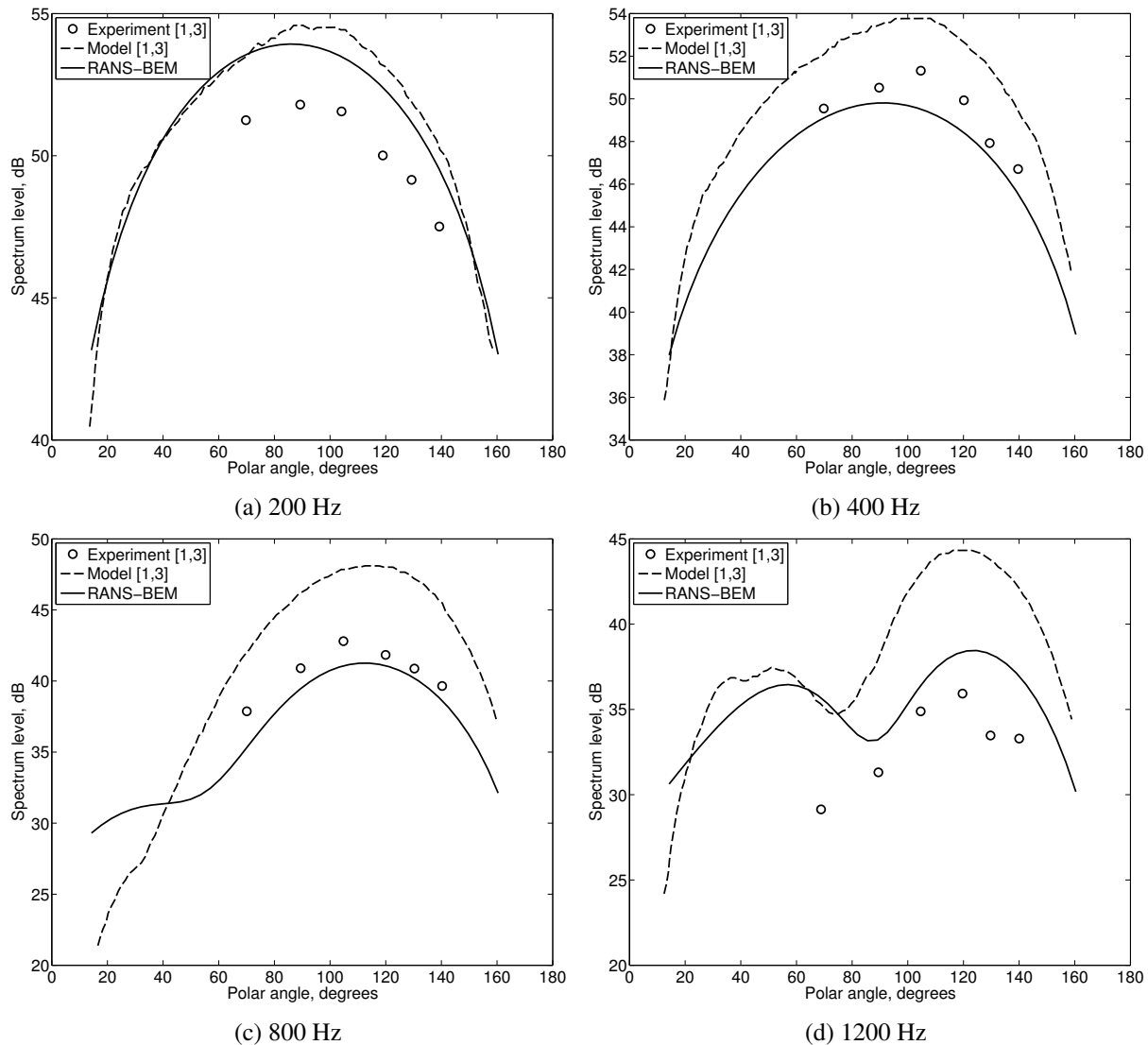
(a) 200 Hz

(b) 400 Hz

(c) 800 Hz

(d) 1200 Hz

Figure 4 – Directivity of the far-field sound spectrum level in dB predicted using the RANS-BEM technique.

[7]  Marburg, S. and Nolte, B., eds., *Computational Acoustics of Noise Propagation in Fluids,* Springer, Berlin, Germany, 2008.

[8]  Kirkup, S. M., *The Boundary Element Method in Acoustics,* Integrated Sound Software, 1998.

[9]  Oberai, A., Roknaldin, F. and Hughes, T. J. R, "Computation of trailing edge noise due to turbulent flow over an airfoil", *AIAA Journal* 40 (2002), pp. 2206–2216.

[10]  Kerhervé, F., Fitzpatrick, J. and Jordan, P., "The frequency dependence of jet turbulence for noise source modelling", *Journal of Sound and Vibration* 296 (2006), pp. 209–225.

[11]  Doolan, C., Albarracin, C. A. and Hansen, C., "Statistical estimation of trailing edge noise", *Proceedings of the 20th International Congress on Acoustics,* Sydney, Australia, 2010.

[12]  Santana, L. D., Schram, C. and Desmet, W., "Airfoil noise prediction from 2data PIV data", *21st AIAA/CEAS Aeroacoustics Conference,* Dallas, Texas, USA, 2015.

[13]  Seo, J.H. and Moon, Y.J., "Aerodynamic noise prediction for long-span bodies", *Journal of Sound and Vibration* 306 (2007), pp. 564–579.

[14]  Corcos, G. M., "The structure of the turbulent pressure field in boundary-layer flows", *Journal of Fluid Mechanics* 18 (1964), pp. 353–378.